IJMMM International Journal of Minerals, Metallurgy and Materials 矿物冶金与材料学报（英文版）

Description of martensitic transformation kinetics in Fe–C–X (X = Ni, Cr, Mn, Si) system by a modified model

Xiyuan Geng, Hongcan Chen, Jingjing Wang, Yu Zhang, Qun Luo, and Qian Li

Cite this article as:
Xiyuan Geng, Hongcan Chen, Jingjing Wang, Yu Zhang, Qun Luo, and Qian Li, Description of martensitic transformation kinetics in Fe–C–X (X = Ni, Cr, Mn, Si) system by a modified model, *Int. J. Miner. Metall. Mater.*, 31(2024), No. 5, pp. 1026-1036. https://doi.org/10.1007/s12613-023-2780-9

Articles you may be interested in

Hai-zhen Wang, Yun-dong Zhao, Yue-hui Ma, and Zhi-yong Gao, Effect of low-energy proton on the microstructure, martensitic transformation and mechanical properties of irradiated Ni-rich TiNi alloy thin films, *Int. J. Miner. Metall. Mater.*, 27(2020), No. 4, pp. 538-543. https://doi.org/10.1007/s12613-019-1893-7

Bing-wei Luo, Jie Zhou, Peng-peng Bai, Shu-qi Zheng, Teng An, and Xiang-li Wen, Comparative study on the corrosion behavior of X52, 3Cr, and 13Cr steel in an O_2-H_2O-CO_2 system:products, reaction kinetics, and pitting sensitivity, *Int. J. Miner. Metall. Mater.*, 24(2017), No. 6, pp. 646-656. https://doi.org/10.1007/s12613-017-1447-9

Richard Espiritu and Alberto Amorsolo Jr., Fabrication and characterization of Cu-Zn-Sn shape memory alloys via an electrodeposition-annealing route, *Int. J. Miner. Metall. Mater.*, 26(2019), No. 11, pp. 1436-1449. https://doi.org/10.1007/s12613-019-1886-6

Sajjad Ali, Yaseen Iqbal, Inamullah Khan, Ansar Ullah, Muhammad Sadiq, Muhammad Fahad, and Khizar Hussain Shah, Hydrometallurgical leaching and kinetic modeling of low-grade manganese ore with banana peel in sulfuric acid, *Int. J. Miner. Metall. Mater.*, 28(2021), No. 2, pp. 193-200. https://doi.org/10.1007/s12613-020-2069-1

Mu-yu Li, Dan Yao, Liu Yang, Hao-ran Wang, and Ying-ping Guan, Kinetic analysis of austenite transformation for B1500HS high-strength steel during continuous heating, *Int. J. Miner. Metall. Mater.*, 27(2020), No. 11, pp. 1508-1516. https://doi.org/10.1007/s12613-020-1979-2

Li Fan, Hai-yan Chen, Yao-hua Dong, Li-hua Dong, and Yan-sheng Yin, Wear and corrosion resistance of laser-cladded Fe-based composite coatings on AISI 4130 steel, *Int. J. Miner. Metall. Mater.*, 25(2018), No. 6, pp. 716-728. https://doi.org/10.1007/s12613-018-1619-2

IJMMM WeChat

QQ author group

INTERNATIONAL JOURNAL OF
Minerals, Metallurgy and Materials

Volume 31, Number 5, May 2024
Page 1026

Research Article https://doi.org/10.1007/s12613-023-2780-9

Description of martensitic transformation kinetics in Fe–C–X (X = Ni, Cr, Mn, Si) system by a modified model

Xiyuan Geng[1)], *Hongcan Chen*[1)], *Jingjing Wang*[2)], *Yu Zhang*[2)], *Qun Luo*[1),✉], *and Qian Li*[1,3,4,5),✉]

1) State Key Laboratory of Advanced Special Steels & Shanghai Key Laboratory of Advanced Ferrometallurgy & School of Materials Science and Engineering, Shanghai University, Shanghai 200444, China
2) Ansteel Beijing Research Institute Co., Ltd, Beijing 102211, China
3) National Engineering Research Center for Magnesium Alloys, Chongqing University, Chongqing 400044, China
4) College of Materials Science and Engineering, Chongqing University, Chongqing 400044, China
5) National Key Laboratory of Advanced Casting Technologies, Chongqing University, Chongqing 400044, China
(Received: 31 August 2023; revised: 1 November 2023; accepted: 6 November 2023)

Abstract: Controlling the content of athermal martensite and retained austenite is important to improving the mechanical properties of high-strength steels, but a mechanism for the accurate description of martensitic transformation during the cooling process must be addressed. At present, frequently used semi-empirical kinetics models suffer from huge errors at the beginning of transformation, and most of them fail to exhibit the sigmoidal shape characteristic of transformation curves. To describe the martensitic transformation process accurately, based on the Magee model, we introduced the changes in the nucleation activation energy of martensite with temperature, which led to the varying nucleation rates of this model during martensitic transformation. According to the calculation results, the relative error of the modified model for the martensitic transformation kinetics curves of Fe–C–X (X = Ni, Cr, Mn, Si) alloys reached 9.5% compared with those measured via the thermal expansion method. The relative error was approximately reduced by two-thirds compared with that of the Magee model. The incorporation of nucleation activation energy into the kinetics model contributes to the improvement of its precision.

Keywords: Fe–C–X system; martensitic transformation; kinetics curve; semi-empirical model; nucleation activation energy

1. Introduction

Advanced high-strength steel (AHSS) has become a highly researched area in the field of automotive structural materials due to its superior strength and ductility [1–2]. Quenching and partitioning (Q&P) steel is a representative of AHSSs, and it exhibits a final microstructure containing martensite and retained austenite, where the retained austenite transforms into martensite during the deformation process, increasing strain hardening and ductility through a transformation-induced plasticity effect [3].

Alloying elements play crucial roles in the microstructural evolution and properties of high-strength steels. The addition of C and Mn lowers the martensite start temperature (M_s) and enhances the thermodynamic stability of austenite, thereby increasing the content of retained austenite after quenching [4–6]. The addition of Mn also improves strength and toughness of high-strength steels. The addition of Ni has been shown to enhance toughness of high-strength steels [7]. The addition of Si suppresses the formation of cementite and destabilizes the retained austenite [8–10]. The inclusion of Cr increases the content of retained austenite by reducing the kinetics of austenite decomposition [11]. Moreover, Cr addition improves the strength and corrosion resistance of high-strength steels [7].

Martensitic transformation of ferrous alloys during quenching can be broadly classified into three categories: athermal, isothermal, and burst transformation. In carbon (C) and low-alloy steels (including Q&P steel), martensite forms at an exceptionally high rate at temperatures below the M_s. Moreover, the content of martensite remains constant at a fixed temperature, with further martensite formation achieved by lowering the temperature. This specific type of martensite is referred to as athermal martensite, with martensitic transformation occurring continuously with the decrease of temperature, i.e., the content of martensitic transformation is a function of temperature.

The mechanical properties of steels can be improved by controlling the proportion of martensite and retained austenite [12]. To achieve such a goal, one must first control the martensite content after the initial quenching at a certain temperature. Therefore, studying the variations in martensite content with temperature during the quenching process, i.e., the kinetics of continuous martensitic transformation, is cru-

✉ Corresponding authors: Qun Luo E-mail: qunluo@shu.edu.cn; Qian Li E-mail: cquliqian@cqu.edu.cn

cial for the composition and process design of AHSSs.

The regulation of martensitic transformation is based on the proposal of an accurate and reasonable kinetics model of continuous martensitic transformation. Several kinetics models have been proposed to describe the martensitic transformation process. However, most of them introduce considerable deviations between the calculation results of kinetics curves and experimental values due to unreasonable assumptions. Moreover, the kinetics curves described by most models exhibit an exponential function shape (C shape), and those of most alloys show a sigmoidal shape (S shape), which may be related to the nucleation of martensite [13]. Therefore, studies should focus on the construction and optimization of kinetics models.

In this work, we provide an overview of the proposed kinetics models and analyze their advantages and limitations. The Magee model was modified by introducing changes in the nucleation activation energy of martensite with temperature. The accuracy of the modified Magee model was validated through the measurement of the martensitic transformation kinetics curves of the Fe–C–X (X = Ni, Cr, Mn, Si) multicomponent system. The calculation error of the modified Magee model decreased substantially, which indicates the rationality of incorporating nucleation activation energy into the kinetics model.

2. Experimental procedures

Fe–C–X alloys were melted from pure elements (Fe: 99.98%, Cr: 99.99%, Mn: 99.99%, Si: 99.99%, and Fe–5wt% C: 99.9%) in an arc-melting vacuum furnace and sucked into a copper mold to obtain cylindrical samples with dimensions of ϕ8 mm × 100 mm. The actual chemical composition of alloys was measured via inductively coupled plasma atomic emission spectrometry and high-frequency infrared C–sulfur analysis (Table 1).

Table 1. Composition of alloys and holding temperatures (HT) during thermal expansion experiments

Alloy	C / at%	Cr / at%	Mn / at%	Si / at%	Fe / at%	HT / K
Fe–C–Cr	0.42	4.90	—	—	Bal.	1223
	0.46	8.71	—	—	Bal.	1223
	0.83	4.86	—	—	Bal.	1223
	1.01	8.26	—	—	Bal.	1223
Fe–C–Mn	0.60	—	4.59	—	Bal.	1173
	0.92	—	1.68	—	Bal.	1173
	0.53	—	2.42	—	Bal.	1173
Fe–C–Mn–Si	1.18	—	2.63	3.03	Bal.	1173
	0.93	—	1.71	3.44	Bal.	1223

The samples were machined into ϕ6 mm × 80 mm cylinders via wire cutting. The thermal expansion curves of samples during quenching were obtained using the thermomechanical simulator Gleeble3500. Each sample was fixed on the jig and heated at a rate of 10 K/s in a resistance heating furnace until the temperature reached 50–100 K above the austenitizing temperature (Table 1). This temperature was held for 5 min to ensure that austenitic transformation occurred completely. The austenitizing temperature was calculated using the thermodynamic database optimized in our previous work [14]. Finally, the samples were cooled to room temperature at a rate of 50 K/s. During the entire thermal expansion period, high-purity Ar (99.999%) gas was continuously introduced to the samples to prevent their oxidation. A thermocouple was spot welded at a central position on the surface of samples to monitor its temperature.

Applying the lever rule [15–16], the thermal expansion curves were transformed into kinetics curves by fitting nonlinear thermal expansion before and after martensitic transformation [17]. The M_s was determined using the 1% offset method for martensite content proposed by Yang and Bhadeshia [18] to reduce the uncertainty of M_s caused by noise. The quenching microstructure was characterized through optical microscopy and scanning electron microscopy (SEM) after polishing and etching with 4vol% nital. With the use of a Sigma 500 field-emission scanning electron microscope, energy dispersive spectrometry (EDS) analysis was carried out to investigate the uniformity of alloy composition. The phase analysis of the quenched alloys was determined via X-ray diffraction (XRD, Bruker D2 Focus) at a scanning range of 35° to 105° and scanning rate of 1.2°/min to determine the content of retained austenite.

3. Review of present kinetics models

The kinetics model of continuous martensitic transformation can be classified into three types: empirical, theoretical, and semi-empirical models. Before modifying the kinetics model, this work provides an overview of several representative models, including their expressions and parameters, as shown in Table 2.

Empirical models are derived by fitting a considerable amount of experimental data, such as martensite volume fraction and M_s, to obtain a phenomenological model applicable to a certain range of alloy compositions without involving the transformation mechanism. Currently, the most widely applied empirical model is that proposed by Koistinen and Marburger (K–M) [19]. They obtained an exponential relationship (K–M model) between the volume fraction of martensite and quenching temperature using experimental data of four C steels with different C contents [19]:

$$f = 1 - \exp[-\alpha \cdot (M_s - T)] \quad (1)$$

Table 2. Summary of continuous martensitic transformation kinetics models

Kinetics model		Expression	Parameters	Notes
Empirical model	K–M [19]	$f = 1 - \exp[-\alpha \cdot (M_s - T)]$	α: rate constant, $\alpha = 0.011$	Limited applicable alloy composition range and low prediction accuracy
	B–S [20]	$f = 1 - \exp[-\alpha \cdot (M_s - T)]$; $\alpha = 0.0224 - 0.0107x_C - 0.0007x_{Mn} - 0.00005x_{Ni} - 0.00012x_{Cr} - 0.0001x_{Mo}$	x_i: weight percentage (wt%) of element i	The same limitations as the K–M model
	Skrotzki [21]	$f = 1 - \left[\frac{T - M_f}{M_s - M_f}\right]^n$	M_f: martensitic finish temperature; n: exponential constant, $n = 2$–3	M_f cannot be calculated directly
Theoretical model	Guimarães and Rios [22]	$f = 1 - \exp\left(-\Gamma\frac{T^* - T}{T}\right)$	T^*: maximum temperature at which martensite embryos can propagate; Γ: lump dimensionless parameter related to the entropy of the martensitic transformation and other physical quantities	Failure to exhibit the S-shaped characteristic of the kinetics curve
Semi-empirical model	Magee [23]	$f = 1 - \exp[-\alpha \cdot (M_s - T)]$; $\alpha = \bar{V}\varphi\frac{d\Delta G^{\gamma\to M}}{dT}$	$\Delta G^{\gamma\to M}$: driving force for the transformation from austenite to martensite; $\bar{V}$: mean volume of martensite; φ: rate constant	The same form as the K–M model with physical significance
	Yu [24]	$f = \frac{M_s - T}{M_s - \beta M_f - (1-\beta)T}$	β: quotient of the entropy of martensite and austenite	Numerous unreasonable assumptions lead to a decrease in predictive accuracy
	Fei *et al.* [25]	$f = \frac{100}{1 + A^{-1}\left(\frac{\Delta G}{100}\right)^{-B}}$; $A = 0.05$; $B = 0.006 \cdot M_s - 0.1369$	ΔG: difference in chemical driving force at T and M_s	The values of A and B lack universality and accuracy
	Power-law [26]	$\frac{\frac{f}{f_{SAT}}}{1 - \frac{f}{f_{SAT}}} = \left(\frac{T^* - T}{T^* - M_s}\right)^\gamma$	f_{SAT}: saturation of the transformation; γ: factor scaling the volume of martensite features	M_s needs to be fitted and deviates significantly from the actual value

where f represents the volume fraction of martensite obtained by measurement of the residual austenite content in alloys via XRD after quenching. T refers to the quenching temperature, and α is a rate constant. α was fitted using the experimental data and is equal to 0.011 for Fe–C alloys. This model was successfully used to predict the martensite transformation curves in low-C steels. However, the rate constant α of the model was assumed to be invariable, which indicates that the type and content of alloying elements had no effect on the kinetics of martensitic transformation but only influenced the value of M_s. The experimental data were only derived from steels with low-C contents and did not account for steels containing higher C content and other alloy elements, which may lead to the nonuniversality of α.

Bohemen and Sietsma [20] quantified the effect of alloying elements on the kinetics of continuous martensitic transformation using experimental data from various steels as a basis. They fitted the experimental data using the K–M model and obtained a series of values of the rate constant α, from which the relationship between α and the alloying elements was derived [20]:

$$\alpha_{BS} = 0.0224 - 0.0107x_C - 0.0007x_{Mn} - 0.00005x_{Ni} - 0.00012x_{Cr} - 0.0001x_{Mo} \quad (2)$$

where x_i represents the weight percentage (wt%) for element i. Substituting Eq. (2) into Eq. (1), the improved K–M model (B–S model) was derived. Eq. (2) reveals the diverse influence of different alloying elements on the kinetics of continuous martensitic transformation. C had the most important influence on kinetics, which may be attributed to its robust solid-solution hardening effect, resulting in strong resistance to the movement of martensite/austenite interfaces [20].

Although Bohemen and Sietsma [20] derived the relationship between rate constant and alloy composition, the accuracy of the model remains to a certain range of compositions. Exceeding the applicable range of compositions would decrease accuracy, which is a common issue for all empirical models [27]. Moreover, the empirical model is a purely phenomenological model and lacks any physical significance; thus, it cannot provide an explanation for the shape of the martensitic transformation curve or transformation process, which limits its development.

Different from empirical models, theoretical models, such as those proposed by Fisher *et al.* [28], Guimarães and Rios [22], Gao *et al.* [29], are derived entirely from the nucleation or growth theory, which can explain the mechanism of martensitic transformation. Guimarães and Rios [22] presented a representative model. They derived the model by analyzing the nucleation and growth of martensite [22]:

$$f = 1 - \exp\left(-\Gamma \frac{T^* - T}{T}\right) \tag{3}$$

where Γ can be theoretically expressed as a function of the mean volume of each martensite plate, changes in entropy during transformation, and so on, and T^* is defined as the highest temperature at which martensite embryos can propagate. This model exhibits certain physical importance. Thus, it can become useful in elucidating the effects of various factors (e.g., composition and prior austenite grain size) on the kinetics of continuous martensitic transformation.

Theoretical models can provide relatively accurate descriptions of the shape of transformation curves; all the parameters involved in the model have explicit physical meaning [30–31]. However, given the unreasonable assumptions regarding the derivation process and as most model parameters cannot be directly obtained, the application of theoretical models is limited.

Semi-empirical models combine theoretical analysis and experimental data; they have a good prediction capability and maintain a certain physical significance of parameters. The earliest semi-empirical model, which was based on the driving force of martensitic transformation, was proposed by Magee [23]. The number of newly formed martensitic plates per unit volume of austenite dN below M_s is suggested to be proportional to the increase in the driving force of martensitic transformation $\Delta G^{\gamma\to M}$ [23]:

$$\mathrm{d}N = -\varphi \Delta G^{\gamma\to M} \tag{4}$$

where φ is a proportionality constant, and the volume fraction of martensite can be expressed as follows [23]:

$$\mathrm{d}f = \bar{V}\mathrm{d}N_V \tag{5}$$

where $\mathrm{d}N_V$ indicates the number of newly formed martensitic plates per volume of the sample, and $\bar{V}$ refers to the average volume of martensitic plates. Evidently, $\mathrm{d}N_V = (1-f)\mathrm{d}N$. Substituting Eq. (4) into Eq. (5) yields the following [23]:

$$\mathrm{d}f = -\bar{V}(1-f)\varphi \frac{\mathrm{d}\Delta G^{\gamma\to M}}{\mathrm{d}T}\mathrm{d}T \tag{6}$$

Integrating Eq. (6) from M_s to T yields the following equation [23]:

$$f = 1 - \exp[-\bar{V}\varphi \frac{\mathrm{d}\Delta G^{\gamma\to M}}{\mathrm{d}T}(M_s - T)] \tag{7}$$

Let $\alpha = \bar{V}\varphi \frac{\mathrm{d}\Delta G^{\gamma\to M}}{\mathrm{d}T}$, then, $f = 1 - \exp[-\alpha\cdot(M_s - T)]$. Thus, this model has the same form as the K–M model. However, α is a simple constant in the K–M model. The Magee model relates α to the driving force for martensitic transformation. The driving force of martensitic transformation differs for alloys of various compositions. The expression of the Magee model explains the relation of α in the K–M model to the composition. Eq. (7) is a development of the K–M model, giving it a certain physical significance.

The semi-empirical model combines theoretical and experimental analyses of martensitic transformation kinetics, making it uniquely advantageous in explaining the martensitic transformation mechanism and predicting kinetics curves. Therefore, the semi-empirical model is the most promising among the three types. However, various semi-empirical models suffer from certain limitations to some extent, such as insufficient description of the martensite nucleation process and assumption of the martensite average volume as a constant. These unreasonable assumptions or analyses will lead to a decrease in the predictive accuracy of the model. Therefore, the physical quantities in the models must be described more accurately to make them more reasonable and predictive.

4. Modification of the kinetics model

Among semi-empirical models, the Magee model was preliminarily used to describe continuous martensitic transformation kinetics due to its simple form, low computational complexity, and utilization of the chemical driving force, which directly connects transformation kinetics to thermodynamics. However, the Magee models assumed the variation rate of the driving force ($\mathrm{d}\Delta G^{\gamma\to M}/\mathrm{d}T$) of martensitic transformation as a constant. However, the driving force of martensitic transformation has an evident nonlinear relationship with temperature. Our previous work [12,14] quantified the driving force of martensitic transformation as the sum of chemical and nonchemical driving forces, where the nonchemical driving force includes the shearing energy of austenite, dilatation strain energy of martensite, and dislocation stored energy. Finally, the driving force of martensitic transformation can be expressed as a function of composition and temperature. Fig. 1 shows the variation rate of the driving force of martensitic transformation for some Fe–C–X (X = Ni, Mn, Si, Cr) alloys with respect to the temperature calculated in this work. The variation rate of the transformation-driving force changed with composition and temperature. The introduction of the variation rate of the driving force into the Magee model would improve the prediction accuracy of the model. However, as the Magee model remains a simple exponential form, the predicted kinetics curve still shows a C shape. Therefore, the S-shaped characteristic of the kinetics curve cannot be exhibited using the original Magee model.

Martensite is nucleated through phonon emission, which

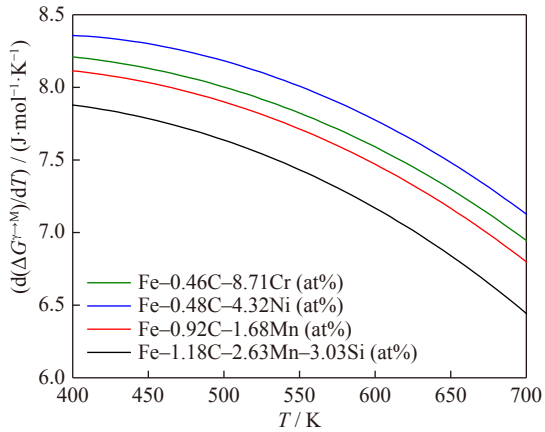

Fig. 1. Variation rate of the driving force of martensitic transformation in Fe–C–X (X = Ni, Mn, Si, Cr) alloys.

requires thermal activation [32]. Thus, in theory, all martensitic transformations are thermally activated. Therefore, for a continuous martensitic transformation kinetics model, the activation energy for nucleation should be considered. Based on this condition, the Magee model can be modified through the incorporation of the thermal activation process, which leads to the following equation:

$$f = 1 - \exp\left[-\bar{V}\varphi \exp\left(-\frac{Q}{RT}\right)\frac{\mathrm{d}\Delta G^{\gamma\to\mathrm{M}}}{\mathrm{d}T}\left(M_\mathrm{s} - T_\mathrm{q}\right)\right] \quad (8)$$

where Q is the activation energy for nucleation, R is the ideal gas constant, and T_q is the quenching temperature. Pati and Cohen [33] observed that the activation energy for the nucleation of martensite decreases monotonically with the decrease in temperature. They derived a linear relationship between the activation energy for nucleation and the driving force, i.e., $Q = A + B\Delta G^{\gamma\to\mathrm{M}}$ [33].

The modified Magee model includes three parameters that need to be estimated through fitting: $\bar{V}\varphi$, A, and B. The S-shaped characteristic of martensitic transformation kinetics curves in Fe–C–X alloys can be described using Eq. (8), which can be a result of the incorporation of temperature-dependent activation energy for nucleation, causing the nucleation rate at different temperatures to change compared with that of the Magee model.

5. Results and discussion

5.1. Microstructure after quenching

Fig. 2 shows the optical micrographs of Fe–C–X (X = Cr, Mn, Si) alloys after quenching. All the alloys presented a typical lath martensite structure, which indicates that the cooling rate of the thermal expansion experiment reached the critical cooling rate for the martensitic transformation of these alloys.

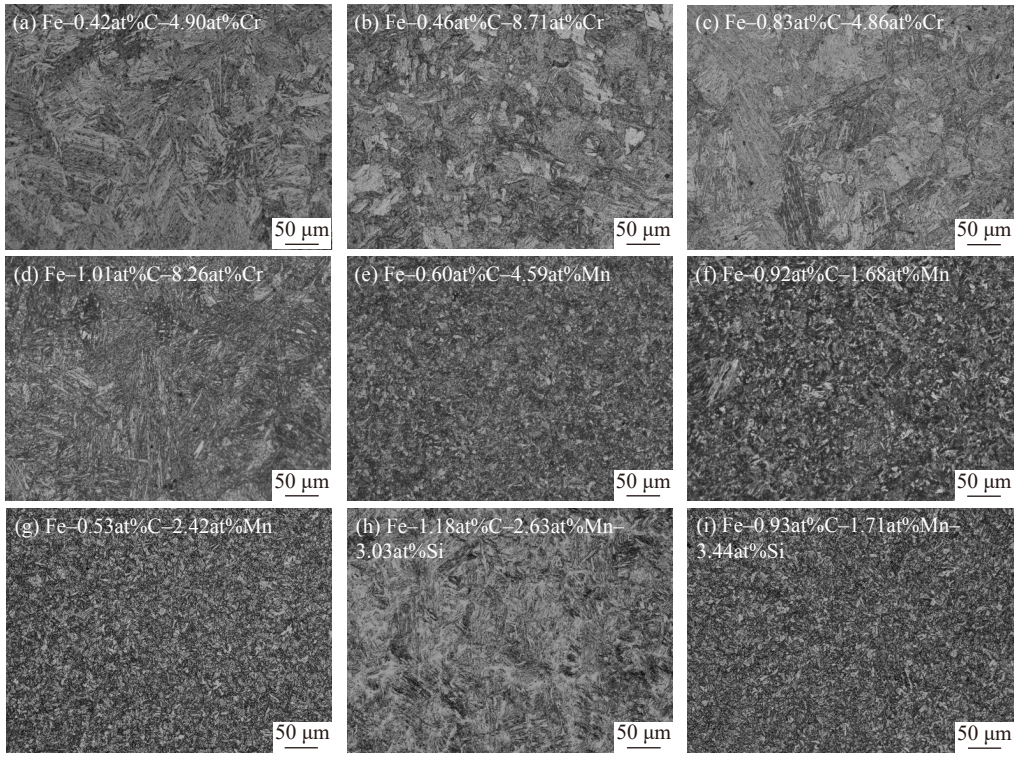

Fig. 2. Optical micrographs of Fe–C–X (X = Cr, Mn, Si) alloys with different compositions after quenching: (a) Fe–0.42at%C–4.90at%Cr; (b) Fe–0.46at%C–8.71at%Cr; (c) Fe–0.83at%C–4.86at%Cr; (d) Fe–1.01at%C–8.26at%Cr; (e) Fe–0.60at%C–4.59at%Mn; (f) Fe–0.92at%C–1.68at%Mn; (g) Fe–0.53at%C–2.42at%Mn; (h) Fe–1.18at%C–2.63at%Mn–3.03at%Si; (i) Fe–0.93at%C–1.71at%Mn–3.44at%Si.

For the observation of fine lath martensite structures, SEM was used to further observe the alloy's microstructure (Fig. 3). The martensite blocks in the alloys consisted of single laths, generally appearing in parallel arrangements. These laths varied in width and length, and some were intersected or truncated by other blocks. Composition measurements using EDS were conducted at three different positions in the alloys after thermal expansion, and the average composition is shown in Table 3. As EDS is insensitive to C, the samples were susceptible to contamination by C-containing substances and other interfering factors, and thus, C was excluded from the EDS results. The elemental content differences at various positions in the tested samples did not exceed 0.3at%, which means that the alloy compositions remained uniform after thermal expansion.

Fig. 4(a) and (b) shows the XRD patterns of Fe–C–Cr and Fe–C–Mn alloys after quenching. The XRD pattern did not show the diffraction peaks of retained austenite or carbide, indicating a relatively complete martensitic transformation. For quaternary alloys, the interaction between elements possibly led to incomplete martensitic transformation, which in turn resulted in the presence of retained austenite after

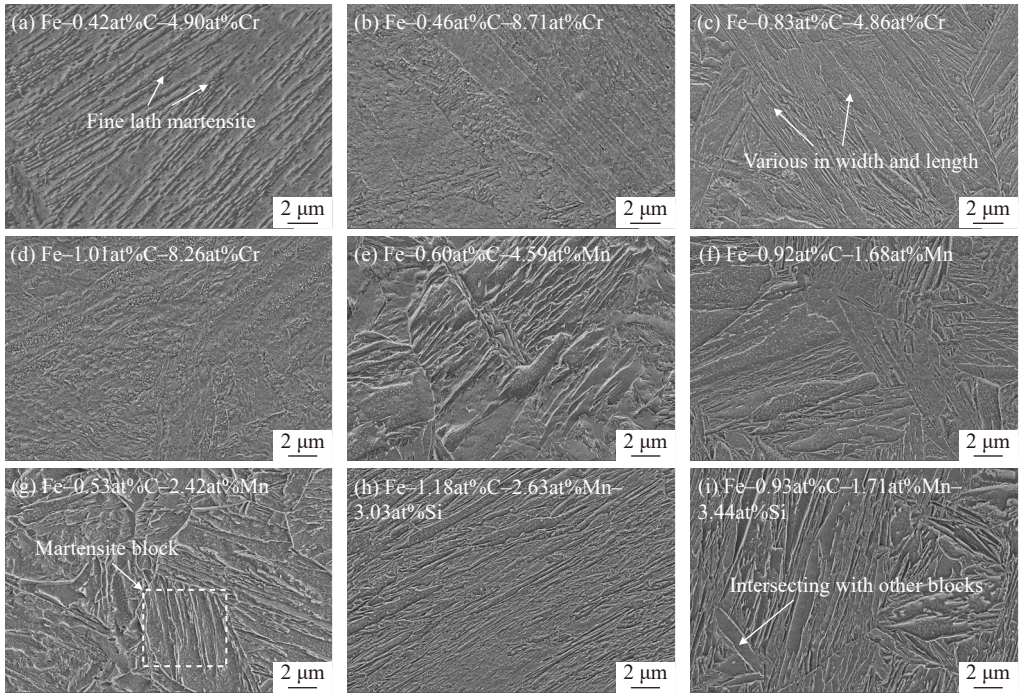

Fig. 3. SEM images of Fe–C–X (X = Cr, Mn, Si) alloys of different compositions after quenching: (a) Fe–0.42at%C–4.90at%Cr; (b) Fe–0.46at%C–8.71at%Cr; (c) Fe–0.83at%C–4.86at%Cr; (d) Fe–1.01at%C–8.26at%Cr; (e) Fe–0.60at%C–4.59at%Mn; (f) Fe–0.92at%C–1.68at%Mn; (g) Fe–0.53at%C–2.42at%Mn; (h) Fe–1.18at%C–2.63at%Mn–3.03at%Si; (i) Fe–0.93at%C–1.71at%Mn–3.44at%Si.

Table 3. EDS results of experimental alloys

Alloy	Fe / at%	Cr / at%	Mn / at%	Si / at%
Fe–0.42at%C–4.90at%Cr	94.3 ± 0.1	5.7 ± 0.1	—	—
Fe–0.46at%C–8.71at%Cr	89.8 ± 0.2	10.2 ± 0.1	—	—
Fe–0.83at%C–4.86at%Cr	94.5 ± 0.2	5.5 ± 0.1	—	—
Fe–1.01at%C–8.26at%Cr	90.1 ± 0.2	9.9 ± 0.1	—	—
Fe–0.60at%C–4.59at%Mn	94.8 ± 0.2	—	5.2 ± 0.2	—
Fe–0.92at%C–1.68at%Mn	97.9 ± 0.2	—	2.1 ± 0.1	—
Fe–0.53at%C–2.42at%Mn	95.7 ± 0.3	—	4.3 ± 0.2	—
Fe–1.18at%C–2.63at%Mn–3.03at%Si	91.0 ± 0.3	—	5.1 ± 0.1	3.9 ± 0.1
Fe–0.93at%C–1.71at%Mn–3.44at%Si	93.7 ± 0.2	—	3.2 ± 0.1	3.1 ± 0.1

quenching. To determine the content of retained austenite, we refined the XRD results. Fig. 4(c) and (d) shows the XRD pattern of Fe–C–Mn–Si alloys after quenching. The black curve represents the original XRD data, the red curve denotes the refined data, and the blue curve is the difference between them. The diffraction pattern revealed weak austenite diffraction peaks, indicating that a certain amount of retained austenite existed in the alloys. The volume fraction of retained austenite (V_γ) can be obtained by the following equation [34]:

$$V_\gamma = 1 - \frac{W_M\left(\frac{a_M^3}{2}\right)}{W_M\left(\frac{a_M^3}{2}\right) + W_\gamma\left(\frac{a_\gamma^3}{4}\right)} \tag{9}$$

where W_M and W_γ refer to the weight percentages of martensite and austenite, respectively. a_M and a_γ are the lattice parameters of martensite and austenite, respectively. All the above parameters were obtained by refining the XRD results. The retained austenite contents of Fe–C–Mn–Si alloys were 7.1 vol% (Fig. 4(c)) and 2.8 vol% (Fig. 4(d)), respectively.

5.2. Martensite transformation kinetics in Fe–C–X (X = Ni, Cr, Mn, Si) system

The thermal expansion curve can reflect the martensitic transformation during the quenching process (Fig. 5), and it can be divided into three stages based on the characteristics of the curve. Before the martensitic transformation, the expansion curve of alloys decreased as the quenching temperature decreased. When martensitic transformation started, the expansion curve began to increase due to the larger volume of martensite compared with austenite, and the rate of increase on the curve gradually rose in the early stage of martensitic transformation and eventually decreased in the later stage. This finding indicates that the transformation rate of martensite followed a similar trend during martensitic

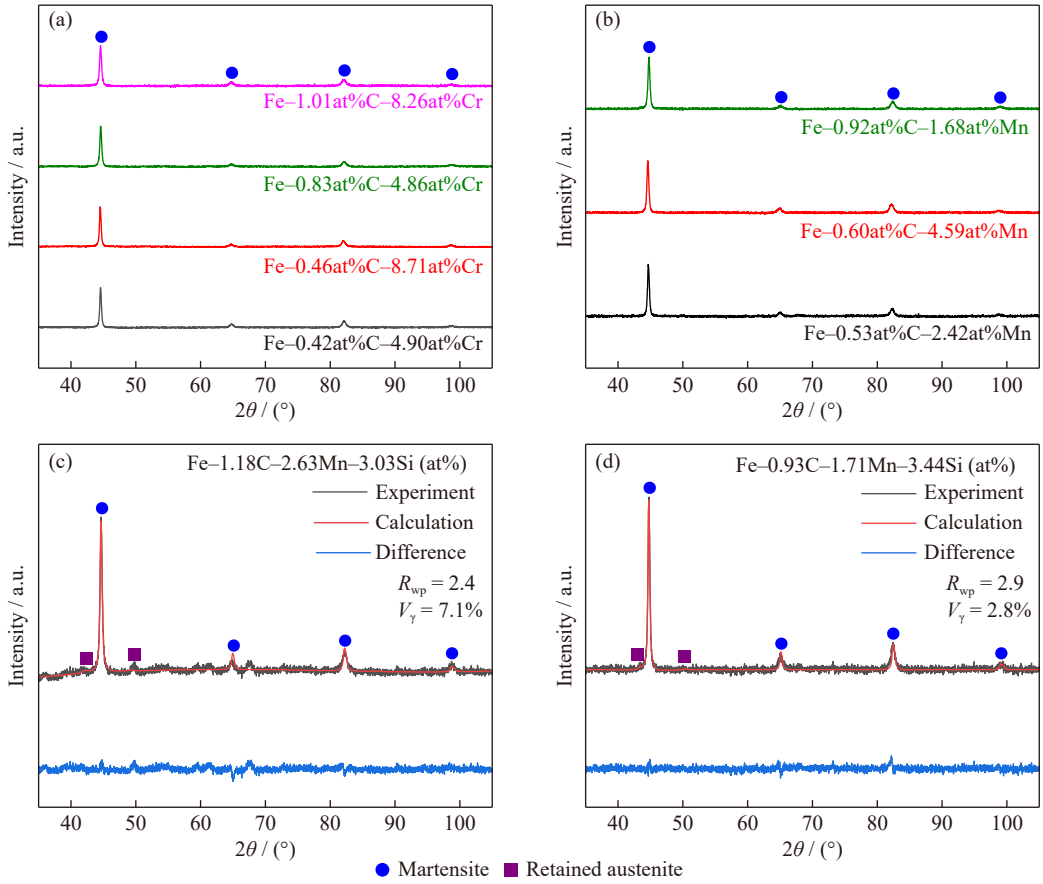

Fig. 4. XRD patterns of (a) Fe–C–Cr, (b) Fe–C–Mn, (c) Fe–1.18C–2.63Mn–3.03Si (at%), and (d) Fe–0.93C–1.71Mn–3.44Si (at%) alloys after quenching. R_{wp} stands for the weighted profile residual factor.

transformation. After the complete martensitic transformation, the expansion curve then continued to decrease with the decrease in quenching temperature. The blue and red lines represent the fitted thermal expansion curves before and after martensitic transformation, respectively. The fitted values closely matched the actual values. The pink line stands for the offset expansion curve of 1% martensite, and M_s can be obtained by identifying the point of intersection between this line and the actual expansion curve.

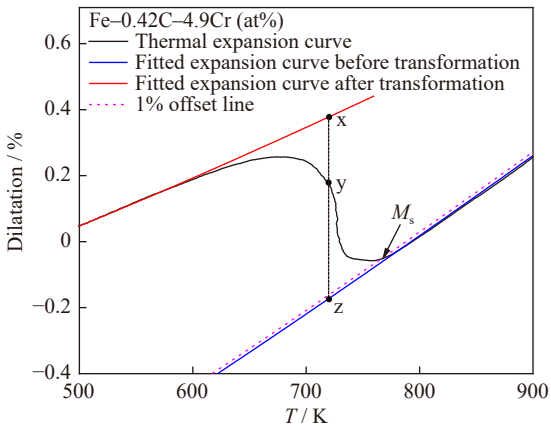

Fig. 5. Thermal expansion curve during the quenching process.

The lever rule is a classic method used to calculate the phase fraction from thermal expansion curves. Assuming an isotropic martensitic transformation, the martensite content is proportional to the dilatation strain. The thermal expansion curves before and after transformation were extrapolated to the temperature range at which transformation occurred (Fig. 5). Based on the relative position of the two extrapolated curves, the martensite content can be calculated using Eq. (10) [15]:

$$f = \frac{\Delta L_{yz}}{\Delta L_{xz}} \tag{10}$$

where ΔL_{yz} is the relative position between the expansion curve and the extrapolated expansion curve before martensitic transformation, ΔL_{xz} is the relative position of the extrapolated expansion curves before and after martensitic transformation. Fig. 6 shows the martensite content versus temperature, i.e., the continuous martensitic transformation kinetics curves obtained using the thermal expansion curve in accordance with the lever rule. As retained austenite was contained in Fe–C–Mn–Si alloys, the martensite content obtained through the lever rule was multiplied by the final martensite content after quenching. All the kinetics curves showed an S shape, and the rate of martensite transformation (the rate of change of martensite content with temperature) increased first and then decreased with the decrease in temperature.

Therefore, continuous martensitic transformation kinetics can be divided into three stages. The first stage featured a low transformation rate because of the relatively high quenching

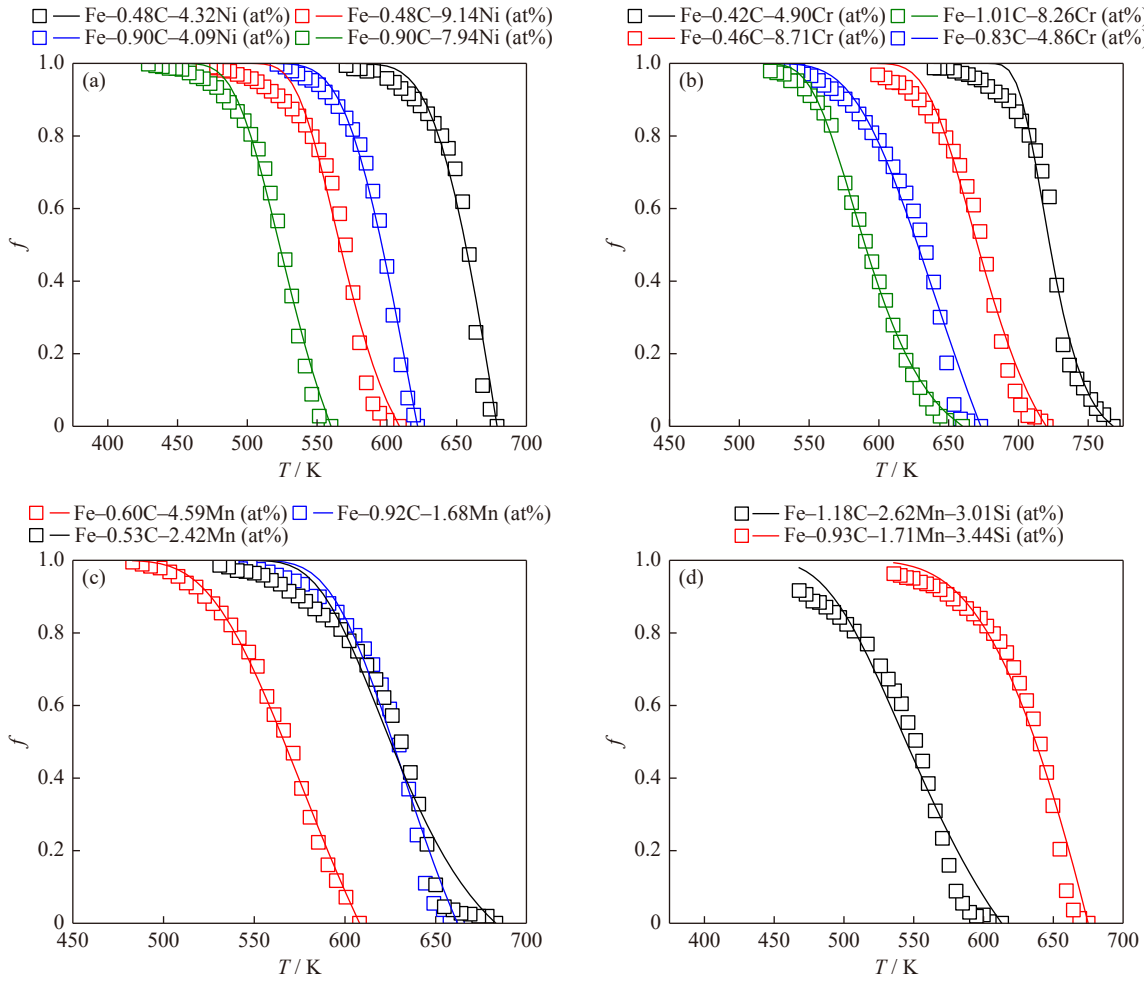

Fig. 6. Continuous martensite transformation kinetics curves of (a) Fe–C–Ni (obtained from our previous work [35]), (b) Fe–C–Cr, (c) Fe–C–Mn, and (d) Fe–C–Mn–Si alloys. The hollow squares represent the experimental values, and the solid curves denote the values calculated using the modified Magee model.

temperature and low driving force of martensitic transformation. As a result, the activated nucleation sites of martensite were few, which led to a low rate of nucleation. With the decrease in quenching temperature, the driving force and the number of nucleation sites of martensite increased. Moreover, the large number of dislocations generated around the formed martensite units provided additional nucleation sites for the following martensite, that is, the autocatalytic nucleation of martensite. As a result, the nucleation rate of martensite rapidly increased due to the combined effect of both factors, thereby increasing the martensitic transformation rate. As the austenite grains were segmented with martensite formation, the average volume of austenite gradually decreased. Thus, the strength of austenite eventually increased, similar to that of fine-grain strengthening. As the martensitic transformation proceeded, austenite was continuously strengthened, its plasticity was hardly adjusted, and the resistance of martensitic transformation increased, which led to the gradual decrease in the martensitic transformation rate until the end of the transformation. Thus, changes in the martensitic transformation rate were controlled by the nucleation rate of martensite and resistance to martensitic transformation. The competition between the nucleation and resistance to transformation caused the martensitic transformation rate to initially increase and then decrease with the decrease in quenching temperature.

5.3. Accuracy of the modified kinetics model

Fig. 6 displays the continuous martensitic transformation kinetics curves of Fe–C–X (X = Ni, Mn, Si, Cr) alloys described using the modified Magee model (Eq. (8)). The martensite contents calculated using the modified Magee model show good agreement with the experimental values. For the Fe–C–X (X = Ni, Cr, Mn, Si) multicomponent system, the calculation error reached 9.5% (the experimental data for martensite fraction $f < 0.05$ were not considered due to the mathematical instability of Eq. (8)). Meanwhile, the shape of kinetics curves described using the modified Magee model was relatively accurate, which cannot be achieved using kinetics models with a simple exponential function form such as the Magee model.

Fig. 7(a) shows the changes in the martensitic transformation rate ($\mathrm{d}f/\mathrm{d}T$) of the martensite fraction of Fe–C–X alloys. The martensitic transformation rate first increased and then decreased with the decrease in temperature. It reached a maximum value at the martensite fraction of approximately 30%.

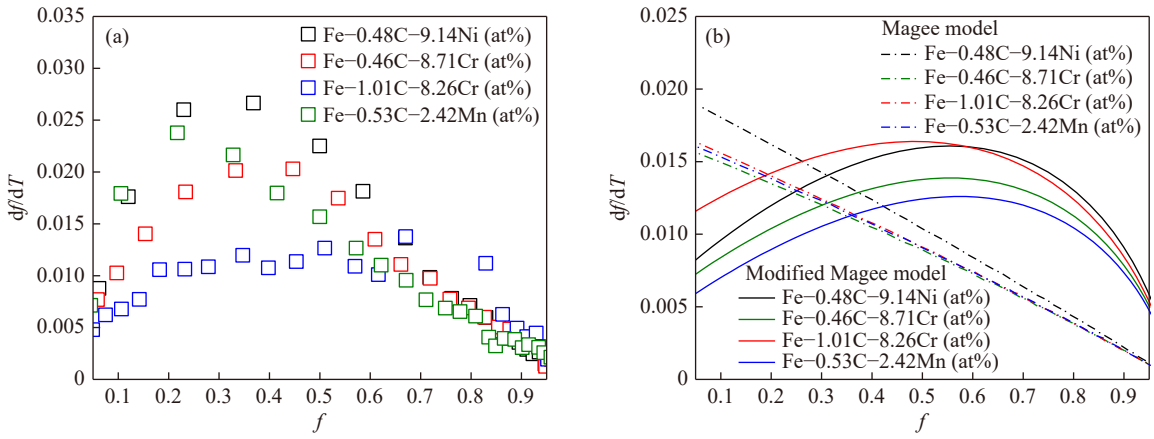

Fig. 7. Changes in martensitic transformation rate (d*f*/d*T*) of martensite fraction: (a) experimental value; (b) calculation results of the Magee model and modified Magee model.

For some alloys, the transformation rate slightly increased in the middle and late stages of transformation, which may be due to excessive heat release during transformation. In addition, heat cannot be dissipated quickly enough, resulting in the rise in the local temperature of the samples, and thus, the increase in the transformation rate. However, the overall transformation rate still increased initially and then decreased. Fig. 7(b) displays the calculation results of the martensitic transformation rate of Fe–C–X alloys observed using the Magee model and modified Magee model. The martensitic transformation rate calculated using the Magee model almost linearly decreased with the increase in transformation fraction, which is inconsistent with the real trend of the transformation rate of Fe–C–X alloys. By contrast, the transformation rate calculated using the modified Magee model increased first and then decreased with the progress of transformation, agreeing with the real trend, due to the introduction of nucleation activation energy into the Magee model. This finding explains the more accurate shape of kinetics curves obtained using the modified Magee model compared with those of the Magee model.

Fig. 8 shows the continuous martensitic transformation kinetics curves calculated using the modified Magee model (Eq. (8)) and other models. The accuracy was greatly improved compared with those of other models. In addition, the S-shaped characteristic of the kinetics curves can be described using the modified Magee model due to the introduction of nucleation activation energy. Notably, the values calculated using the power-law model are also in good agreement with the experimental findings. The values of M_s fitted by the power-law model deviated considerably from the experimental findings, which resulted in a loss of physical significance and did not promote the understanding of the actual process. On the other hand, if the experimental values of M_s were used, a substantial decrease in the calculation accuracy of the kinetics curves would have been observed.

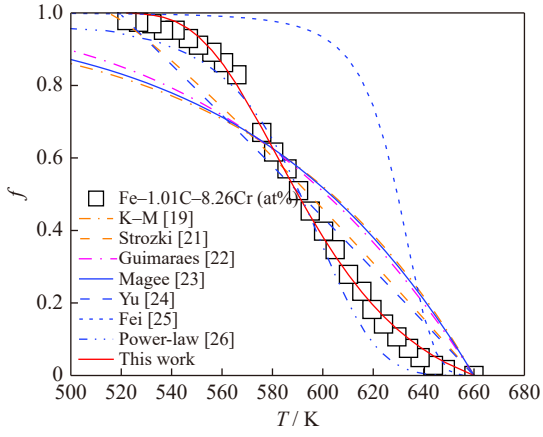

Fig. 8. Calculation results of continuous martensite transformation kinetics curves obtained using the modified Magee model and other models [19,21–26].

Given the fixed rate constant of the K–M and Magee models at various quenching temperatures, the nucleation rate of martensite remained constant during martensitic transformation. However, the nucleation rate of martensite varied with the progress of martensitic transformation, which explains the low accuracy of the two models. The introduction of nucleation activation energy to the kinetics model led to changes in the nucleation rate of martensite with temperature, thereby improving the accuracy of the model. Furthermore, the S-shaped characteristic of the kinetics curve depicted using the modified Magee model demonstrated that the model is more reasonable and suitable compared with the others.

Table 4 shows the calculation errors of the kinetics curves of Fe–C–X (X = Ni, Cr, Mn, Si) alloys (Fig. 6) during continuous martensitic transformation when using different kinetics models. The calculation accuracy of the modified Magee model is evidently higher than those of the Magee model and other models. Therefore, the changes in nucle-

Table 4. Calculation error of kinetics models of continuous martensitic transformation [19,21–24]

Kinetics model	Calculation error / %
K–M [19]	33.5
Guimarães and Rios [22]	29.2
Skrotzki [21]	19.4
Yu [24]	21.1
Magee [23]	30.2
Modified Magee	9.5

ation activation energy of martensite with temperature must be considered in the kinetics model.

However, compared with experimental values, the martensitic transformation process observed using the current modified model showed a large deviation in the late stage of transformation. The deviation may be related to the limitations that may still exist in the modified model. As austenite grains were continuously divided by martensite units during transformation, the subsequently formed martensite units contained a small austenite volume, resulting in the decreased average volume of martensite with the decrease in quenching temperature. By contrast, the average volume of martensite is regarded as a constant in the current modified model, which needs to be improved. Moreover, the growth of martensite may involve a thermal activation process [36–37]; however, only the thermal activation process of nucleation is considered in the current modified model. Therefore, the introduction of the thermal activation process of martensite growth into the model may improve its accuracy and can be considered in the following work. Nonetheless, the introduction of nucleation activation energy improved the accuracy of the kinetics model, indicating that nucleation activation energy should be considered in the martensitic transformation process, which constitutes the significance of our work.

6. Conclusion

A modified kinetics model was proposed by introducing the nucleation activation energy of martensite, which changes with temperature, into the Magee model. As a result, varying nucleation rates were observed during martensitic transformation. The kinetics curves of martensitic transformation in Fe–C–X (X =Ni, Cr, Mn, Si) alloys were described using the modified model, and the calculation error was 9.5%, which is evidently lower than those of the Magee model and other kinetics models. The S-shaped characteristic of the kinetics curve of martensitic transformation can be described using the modified model, with the calculated values of the martensitic transformation rate showing good agreement with experimental values. The improved accuracy of the modified model proves the necessity of considering nucleation activation energy in martensitic transformation.

Acknowledgements

This work was financially supported by the National Natural Science Foundation of China (No. U2102212) and the Shanghai Rising-Star Program (No. 21QA1403200).

Conflict of Interest

Qian Li is an editorial board member for this journal and was not involved in the editorial review or the decision to publish this article. The authors declare that they have no financial interests or personal relationships that could have appeared to influence the work reported in this paper.

References

[1] C. Yao, M. Wang, Y.J. Ni, *et al*., Effect of traveling-wave magnetic field on dendrite growth of high-strength steel slab: Industrial trials and numerical simulation, *Int. J. Miner. Metall. Mater.*, 30(2023), No. 9, p. 1716.

[2] W.L. Wang, L.K. Wang, and P.S. Lyu, Kinetics of austenite growth and bainite transformation during reheating and cooling treatments of high strength microalloyed steel produced by sub-rapid solidification, *Int. J. Miner. Metall. Mater.*, 30(2023), No. 2, p. 354.

[3] X.Y. Yuan, Y. Wu, X.J. Liu, H. Wang, S.H. Jiang, and Z.P. Lü, Revealing the role of local shear strain partition of transformable particles in a TRIP-reinforced bulk metallic glass composite via digital image correlation, *Int. J. Miner. Metall. Mater.*, 29(2022), No. 4, p. 807.

[4] E. De Moor, J.G. Speer, D.K. Matlock, J.H. Kwak, and S.B. Lee, Quenching and partitioning of CMnSi steels containing elevated manganese levels, *Steel Res. Int.*, 83(2012), No. 4, p. 322.

[5] F. HajyAkbary, J. Sietsma, G. Miyamoto, T. Furuhara, and M.J. Santofimia, Interaction of carbon partitioning, carbide precipitation and bainite formation during the Q&P process in a low C steel, *Acta Mater.*, 104(2016), p. 72.

[6] J. Kähkönen, D.T. Pierce, J.G. Speer, *et al*., Quenched and partitioned CMnSi steels containing 0.3wt.% and 0.4wt.% carbon, *JOM*, 68(2016), No. 1, p. 210.

[7] L. Wang, C.F. Dong, C. Man, Y.B. Hu, Q. Yu, and X.G. Li, Effect of microstructure on corrosion behavior of high strength martensite steel—A literature review, *Int. J. Miner. Metall. Mater.*, 28(2021), No. 5, p. 754.

[8] G. Miyamoto, J. Oh, K. Hono, T. Furuhara, and T. Maki, Effect of partitioning of Mn and Si on the growth kinetics of cementite in tempered Fe–0.6 mass% C martensite, *Acta Mater.*, 55(2007), No. 15, p. 5027.

[9] Y. Toji, H. Matsuda, M. Herbig, P.P. Choi, and D. Raabe, Atomic-scale analysis of carbon partitioning between martensite and austenite by atom probe tomography and correlative transmission electron microscopy, *Acta Mater.*, 65(2014), p. 215.

[10] P.F. Gao, F. Li, K. An, Z.Z. Zhao, X.H. Chu, and H. Cui, Microstructure and deformation mechanism of Si-strengthened intercritically annealed quenching and partitioning steels, *Mater. Charact.*, 191(2022), art. No. 112145.

[11] D.T. Pierce, D.R. Coughlin, K.D. Clarke, *et al*., Microstructural evolution during quenching and partitioning of 0.2C–1.5Mn–1.3Si steels with Cr or Ni additions, *Acta Mater.*, 151(2018), p. 454.

[12] Q. Luo, H.C. Chen, W. Chen, C.C. Wang, W. Xu, and Q. Li, Thermodynamic prediction of martensitic transformation temperature in Fe–Ni–C system, *Scripta Mater.*, 187(2020), p. 413.

[13] Y. Li, L.Y. Wang, K.Y. Zhu, C.C. Wang and W. Xu, An integral transformation model for the combined calculation of key martensitic transformation temperatures and martensite fraction, *Mater. Des.*, 219(2022), art. No. 110768.

[14] H.C. Chen, W. Xu, Q. Luo, *et al*., Thermodynamic prediction of martensitic transformation temperature in Fe–C–X (X=Ni, Mn, Si, Cr) systems with dilatational coefficient model, *J. Mater. Sci. Technol.*, 112(2022), p. 291.

[15] L.H. Liu and B. Guo, Dilatometric analysis and kinetics research of martensitic transformation under a temperature gradient and stress, *Materials*, 14(2021), No. 23, art. No. 7271.

[16] M.Y. Li, D. Yao, L. Yang, H.R. Wang, and Y.P. Guan, Kinetic analysis of austenite transformation for B1500HS high-strength steel during continuous heating, *Int. J. Miner. Metall. Mater.*, 27(2020), No. 11, p. 1508.

[17] S.M.C. van Bohemen, The nonlinear lattice expansion of iron alloys in the range 100–1600K, *Scripta Mater.*, 69(2013), No. 4, p. 315.
[18] H.S. Yang and H.K.D.H. Bhadeshia, Uncertainties in dilatometric determination of martensite start temperature, *Mater. Sci. Technol.*, 23(2007), No. 5, p. 556.
[19] D.P. Koistinen and R.E. Marburger, A general equation prescribing the extent of the austenite-martensite transformation in pure iron–carbon alloys and plain carbon steels, *Acta Metall.*, 7(1959), No. 1, p. 59.
[20] S.M.C. van Bohemen and J. Sietsma, Effect of composition on kinetics of athermal martensite formation in plain carbon steels, *Mater. Sci. Technol.*, 25(2009), No. 8, p. 1009.
[21] B. Skrotzki, The course of the volume fraction of martensite vs. temperature function $M_x(T)$, *J. Phys. IV France*, 1(1991), No. C4, p. 367.
[22] J.R.C. Guimarães and P.R. Rios, Modeling lath martensite transformation curve, *Metall. Mater. Trans. A*, 44(2013), No. 1, p. 2.
[23] C.L. Magee, The nucleation of martensite, [in] H.I. Aaronson and V.F. Zackay, eds., *Phase Transformations*, ASM International, Materials Park, Ohio, 1970.
[24] H.Y. Yu, A new model for the volume fraction of martensitic transformations, *Metall. Mater. Trans. A*, 28(1997), No. 12, p. 2499.
[25] H.Y. Fei, P. Hedström, L. Höglund, and A. Borgenstam, A thermodynamic-based model to predict the fraction of martensite in steels, *Metall. Mater. Trans. A*, 47(2016), No. 9, p. 4404.
[26] J.R.C. Guimarães, P.R. Rios, and A.L.M. Alves, Power-law description of martensite transformation curves, *Mater. Sci. Technol.*, 37(2021), No. 17, p. 1362.
[27] B. Nenchev, Q. Tao, Z.H. Dong, *et al*., Evaluating data-driven algorithms for predicting mechanical properties with small datasets: A case study on gear steel hardenability, *Int. J. Miner. Metall. Mater.*, 29(2022), No. 4, p. 836.
[28] J.C. Fisher, J.H. Hollomon, and D. Turnbull, Kinetics of the austenite→martensite transformation, *JOM*, 1(1949), No. 10, p. 691.
[29] Q.Z. Gao, C. Wang, F. Qu, Y.L. Wang, and Z.X. Qiao, Martensite transformation kinetics in 9Cr–1.7W–0.4Mo–Co ferritic steel, *J. Alloys Compd.*, 610(2014), p. 322.
[30] K. Chou, General solution model and its new progress, *Int. J. Miner. Metall. Mater.*, 29(2022), No. 4, p. 577.
[31] X.Y. Liu, F.Y. Sun, W. Wang, *et al*., Effect of chromium interlayer thickness on interfacial thermal conductance across copper/diamond interface, *Int. J. Miner. Metall. Mater.*, 29(2022), No. 11, p. 2020.
[32] M. Hong, K. Wang, Y.Z. Chen, and F. Liu, A thermo-kinetic model for martensitic transformation kinetics in low-alloy steels, *J. Alloys Compd.*, 647(2015), p. 763.
[33] S.R. Pati and M. Cohen, Nucleation of the isothermal martensitic transformation, *Acta Metall.*, 17(1969), No. 3, p. 189.
[34] E.J. Pickering, J. Collins, A. Stark, L.D. Connor, A.A. Kiely, and H.J. Stone, *In situ* observations of continuous cooling transformations in low alloy steels, *Mater. Charact.*, 165(2020), art. No. 110355.
[35] W. Chen, H.C. Chen, C.C. Wang, *et al*., Effect of dilatational strain energy of Fe–C–Ni system on martensitic transformation, *Acta Metall. Sin.*, 58(2022), No. 2, p. 175.
[36] J.R.C. Guimarães and P.R. Rios, Microstructural path analysis of martensite dimensions in FeNiC and FeC alloys, *Mater. Res.*, 18(2015), No. 3, p. 595.
[37] P.R. Rios and J.R.C. Guimarães, Athermal martensite transformation curve, *Mater. Res.*, 19(2016), No. 2, p. 490.